Pergamon

Ann. Nucl. Energy, Vol. 25, No. 11, pp. 859–888, 1998

PII: S0306-4549(98)00001-2
Printed in Great Britain
0306-4549/98 $19.00 + 0.00

Thermal Hydrodynamical Analysis of a Countercurrent Gas Centrifuge

D. A. de Andrade, J. L. F. Bastos

Instituto de Pesquisas Energéticas e Nucleares (IPEN/CNEN-SP)

Divisão de Termo Hidráulica (RAT)

Travessa R, 400 - Cidade Universitária

Caixa Postal 11.049; CEP 05422-970; São Paulo - SP - Brazil

E-mail: delvonei@net.ipen.br

(Received 2 October 1997)

Abstract—The separative effect in a centrifuge is amplified when a countercurrent in the axial direction is added to the centrifugal field. The mchanisms used to create this countercurrent are obtained with the gas deceleration near to the waste scoop, mechanical effect, and temperature distribution on the rotor walls, thermal effect. This work treats the influence of the thermal countercurrent on the centrifuge separative performance. A complete centrifuge model is presented, therefore this study passes by the hydrodynamical and thermal phenomena analysis. For the accomplishment of this work the gas flow is simulated inside the rotor, initially with arbitrary thermal boundary conditions. Then a structural thermal model is developed to supply the realistic boundary conditions for the hydrodynamical model. This procedure, with the integrated models, allows to propose and to evaluate configuration changes for a centrifuge minimizing the laboratory phase tests.

Introduction

The idea of using centrifugal or gravitational fields to separate a mixture of gases of different molecular weights is very old. In 1895 experiments for this purpose were driven in Germany. The use of this principle to achieve significant separation of uranium isotopes began in United States during The Second World War with the purpose of producing enriched uranium for the program of atomic weapons. After The Second World War, several countries concentrated their efforts to the research and development in centrifugation in view of new applications as the production of fuel for light water reactors. Improvements in the size, velocity and efficiency of the centrifuges were reached in Germany that, in 1958 built machines to separate argon isotopes. Zippe (1960) conducted experiments in centrifugation in USSR, USA and Germany and developed the light and durable centrifuge from which modern projects descended. Starting from the experimental program of Zippe at the University of Virginia, programs for plants implementation began in United States and in Germany for industrial production of enriched uranium by the centrifugation process. In 1960, the North American Commission of Atomic Energy decided to prohibit the publication of any technical or operational information related to the centrifuges in development in United States. The same line was followed later in Germany, in England and in Holland. Since then, the only information published on the subject was exclusively of theoretical or informative character. Also in 1960, the centrifugation process began to be investigated in Japan and it was instituted as being the national project for uranium enrichment. In 1970 the Federal Republic of Germany, England and Holland, by means of the Almelo's Agreement, created the consortium URENCO/CENTEC with the purpose of accomplishing the development of the gas centrifuge process in industrial scale.

In Brazil, the studies on isotope enrichment started in 1958 in a purely academic character. By the end of the 70's a research program started aiming at the development of a centrifuge model for uranium enrichment in industrial scale. Several prototypes were built and tested. The current models present compatible performances with similar machines around the world and our studies are oriented now to improve the separation performance and cost reduction.

Gas Centrifuge Functioning Principle

A centrifuge, Figure 1, is constituted by a recipient, shell, with a vertical cylinder in its interior, rotor. This cylinder rotates at very high velocities. The physics of the flow is described in several works Stewartson (1957); Greenspan (1969); Sakurai (1974); Bark (1976). The rotor can be supported on a metallic needle or can be suspended by electromagnetic bearings. The region between the rotor and shell is maintained under vacuum by a turbomolecular pump. A tubular axis in the center of the rotor is used for the introduction of the feeding mixture, UF_6. The extraction of the product, $^{235}UF_6$, and waste, $^{238}UF_6$, is done by collector tubes, called scoops. The motor is positioned in the lower part between the rotor and shell. The separation of the light isotope from the heavy isotope is obtained with the centrifugal field generated by the rotor that establishes a pressure distribution on the gaseous isotope mixture. This pressure distribution manifested in the form of a radial increase of pressure is different for the different isotopes of the mixture since the action of the centrifugal field depends on the mass. However, the separation resulted by the action of the centrifugal field is very limited. An additional separative effect is obtained with the generation of a countercurrent in the axial direction. This countercurrent is a result of the composition of two mechanisms:

- deceleration of the gas in one of the extremities of the rotor (mechanical countercurrent);
- distribution of temperatures on the rotor walls (thermal countercurrent).

The mechanical countercurrent is obtained by positioning the waste scoop in one of the rotor extremities, which generates a flow deceleration, associated with a rotating disk in the opposite extremity. The thermal countercurrent is obtained by the gradient of temperatures on the rotor walls. Centrifuges that use this separative principle are also denominated as "Countercurrent Centrifuges."

The separation capacity of a centrifuge is given by two categories of variables: the separation parameters (separation , stripping and enriching factors) and the flow parameters (feeding , product and waste flows). None of these parameters separately allows to check the separative performance of a centrifuge. In order to have an efficient machine, we should have a high separation factor and a high feeding flow. The parameter that quantifies the separative performance of a centrifuge is denominated Separative Capacity, δU, that takes simultaneously into account the separation and flow parameters. Although δU has no physical meaning, this parameter is

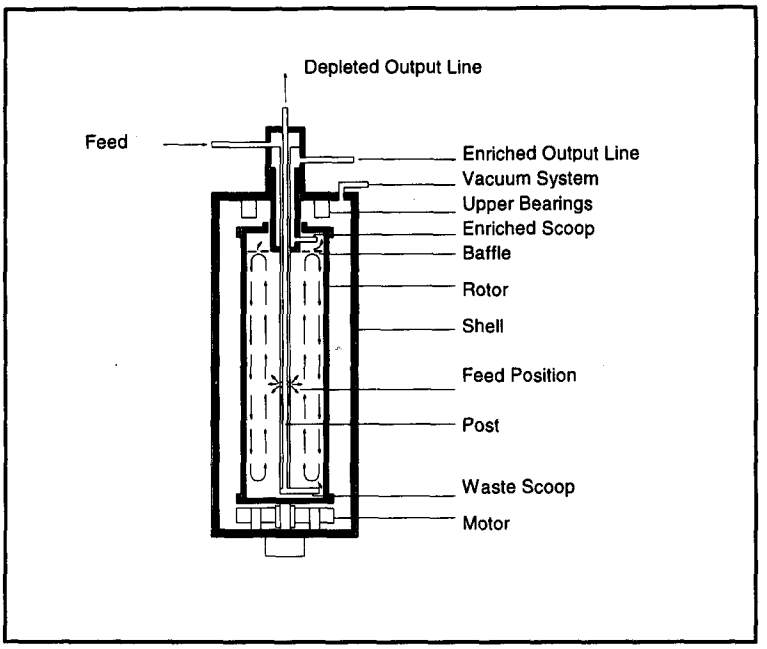

Figure 1 - Schematic representation of a Gas Centrifuge

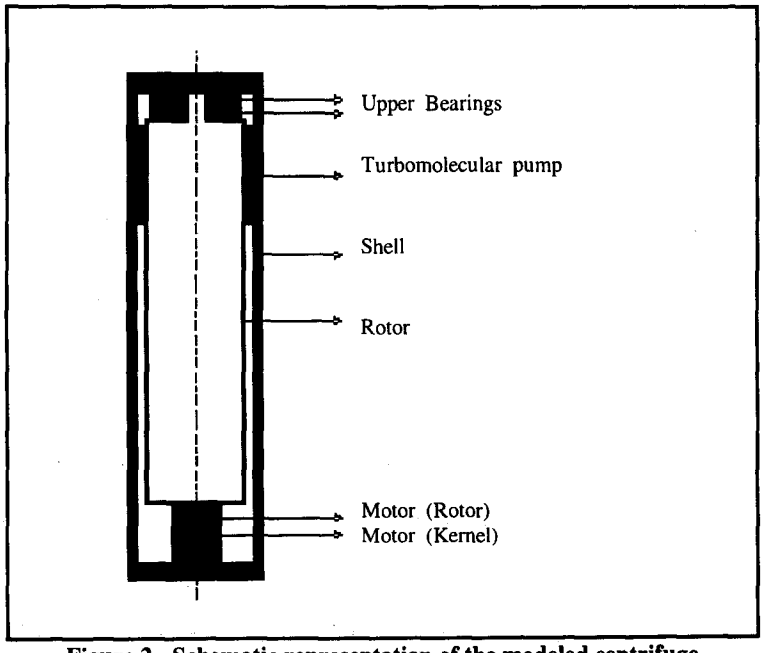

Figure 2 - Schematic representation of the modeled centrifuge

convenient because it can be calculated from measured variables in the laboratory. The unit of δU is SWU/year, Separative Work Unit per year.

Description of the adopted model

Figure 2 is a schematic representation of the modeled centrifuge. The main components are:

Rotor - internal cylinder which rotates at high velocities and it contains the gas, UF_6;

Shell - external cylinder which is the structural support for the turbomolecular pump and other components;

Motor - responsible for the movement of the rotor;

Upper Bearings - responsible for rotor stability and to maintain it suspended without physical contact with any other component of the centrifuge by the generation of an electromagnetic field;

Turbomolecular Pump- maintains under vacuum the region between the rotor and shell.

The feeding and withdrawal systems are not represented physically in the model. This simplification is denominated "total reflux".

The centrifuge was assumed with shell in steel and rotor in treated steel, Maraging, to resist high tensions. The turbomolecular pump is in aluminum. The motor is divided in two parts. The structure of the internal part is in pure aluminum wrapped up with copper wiring covered by resin. The external part of the motor is in Maraging.

Flow modeling

The UF_6 flow inside the rotor is governed by the mass, momentum and energy equations for a compressible flow in cylindrical geometry and the state equation for perfect gas, equations 1 to 6. The hypotheses considered are: steady state, laminar compressible flow, constant physical properties and axial symmetry.

$$\frac{\partial}{\partial z}(\rho V_z)+\frac{1}{r}\frac{\partial}{\partial r}(\rho r V_r)=0 \qquad (1)$$

$$\rho\left(V_z\frac{\partial V_z}{\partial z}+V_r\frac{\partial V_z}{\partial r}\right)=-\frac{\partial p}{\partial z}+\mu\left(\nabla^2 V_z+\frac{1}{3}\frac{\partial}{\partial z}divV\right) \tag{2}$$

$$\rho\left(V_z\frac{\partial V_r}{\partial z}+V_r\frac{\partial V_r}{\partial r}-\frac{V_\theta^2}{r}\right)=-\frac{\partial p}{\partial r}+\mu\left[\left(\nabla^2-\frac{1}{r^2}\right)V_r+\frac{1}{3}\frac{\partial}{\partial r}divV\right] \tag{3}$$

$$\rho\left(V_z\frac{\partial V_\theta}{\partial z}+V_r\frac{\partial V_\theta}{\partial r}+\frac{V_r V_\theta}{r}\right)=\mu\left(\nabla^2-\frac{1}{r^2}\right)V_\theta \tag{4}$$

$$\rho C_v\left(V_z\frac{\partial T}{\partial z}+V_r\frac{\partial T}{\partial r}\right)+pdivV=k\nabla^2 T+\Phi_{visc} \tag{5}$$

where:

$$\Phi_{visc}=2\mu\left\{\left(\frac{\partial V_z}{\partial z}\right)^2+\left(\frac{\partial V_r}{\partial r}\right)^2+\frac{V_r^2}{r^2}+\frac{1}{2}\left[\left(\frac{\partial V_\theta}{\partial z}\right)^2+\left(\frac{\partial V_r}{\partial z}+\frac{\partial V_z}{\partial r}\right)^2+\left(\frac{\partial V_\theta}{\partial r}+\frac{V_\theta}{r}\right)^2-\frac{1}{3}(divV)^2\right]\right\} \tag{5a}$$

$$divV=\frac{\partial V_z}{\partial z}+\frac{1}{r}\frac{\partial(rV_r)}{\partial r}, \tag{5b}$$

$$\nabla^2=\frac{\partial^2}{\partial z^2}+\frac{\partial^2}{\partial r^2}+\frac{1}{r}\frac{\partial}{\partial r}, \tag{5c}$$

$$p=\frac{R}{M}\rho T. \tag{6}$$

Expression for the Separative Capacity δU

There are different methods to calculate δU for total reflux models. In this work it was adopted an extension of the of the Cohen radial averages method proposed by Soubbaramayer (1979). For low concentrations δU can be expressed by equation (7):

$$\delta U=\frac{1}{2}F\theta(1-\theta)\left[\frac{q-1}{1+(q-1)\theta}\right]^2 \tag{7}$$

In this expression, F is the feeding flow, θ is the ratio between the product and waste flows (cut) and q is the enrichment factor. The expression of q takes into account the axial flow of mass, ρV_z , coming of the flow calculation. The mechanical countercurrent is generated by the deceleration of the gas near to the waste collector. This effect is essentially three-dimensional and it depends on the geometry of the collector. In the bidimensional model adopted, the effect of the scoop on the flow is reproduced by a rotating disk with an angular velocity smaller than the angular velocity of the rotor, figure 3. In this work an analysis is presented corresponding to a deceleration of 10% compared to the rotor velocity: $\Delta\Omega = 0.1\Omega$.

Boundary Conditions

The boundary conditions are:

On the upper cover of the rotor: prescribed velocity and temperature.

On the lower cover of the rotor: prescribed velocity and temperature.

On the axis of the centrifuge, symmetry conditions for the velocity and temperature fields.

Numerical Method

The numerical solution of the conservation equations was accomplished with the Finite Volume Method by Maliska and collaborators (1992). Special attention was given to the coupling of pressure and velocity due to convergence problems observed for the cases of higher rotations. A variant of the SIMPLE method was used, Maliska (1995).

Due to the high centrifugal field established inside the rotor, it is expected that most of the gas is concentrated in a close area near to the side wall. For the angular velocities of interest, the layer where the countercurrent occurs is of the order of millimetres. So, it is expected that there is a large region where the density is very low, central region, and other of high densities, close to the wall. This fact suggests the construction of meshes quite deformed with high control volumes concentration close to the lateral wall of the

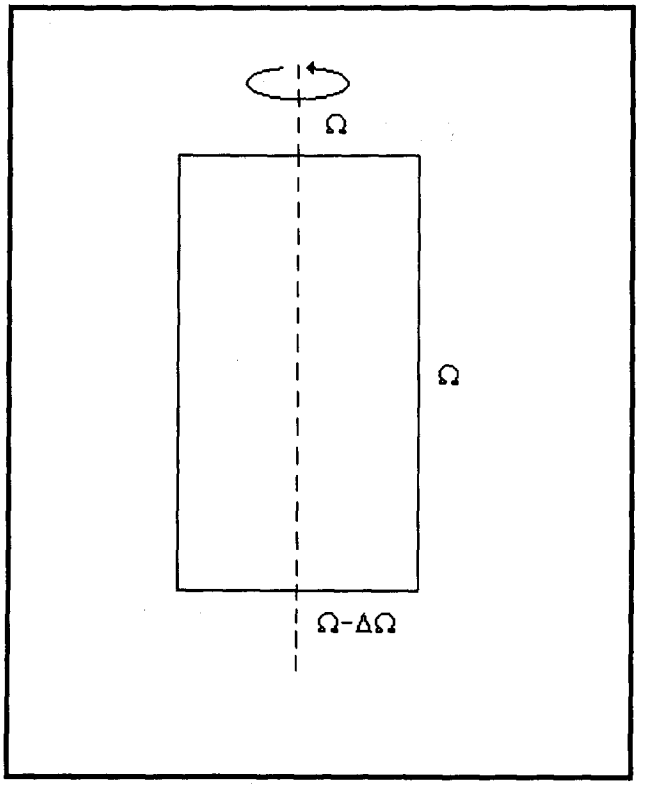

Figure 3 - Outline of the treated geometry

rotor. A typical mesh for this problem is presented in Figure 4.

Results of the Hydrodynamical Model

The first case analyzed corresponds to a situation where the whole rotor is maintained at a constant temperature TSB=308 K. This way, there is no convective effect due to temperature gradients on the covers and lateral wall of the cylinder. Only the effect of the mechanical countercurrent is present.

Figure 5 presents the densities field in dimensionless coordinates Z/H and R/Rw, where H is the total height of the rotor and Rw the rotor radius. It is noticed that in the center of the cylinder, the densities are very low, black area, assuming larger values as it approaches the lateral wall of the cylinder. The highest values are represented by the white area and they appear close to the wall. This density stratification is explained by the action of the centrifugal field. This result confirms the results of the literature which affirm that practically the whole mass of the gas is in a fine layer close to the lateral wall of the rotor.

Figure 6 presents the stream lines. The stream lines appear from a dimensionless radius of 0.76 and concentrate on the right lower corner indicating that the whole mass contained in the rotor passes by this area.

Figure 7 presents the velocities field. Close to the upper cover the gas is accelerated and the velocities are in the direction from the center to the wall. In the area of the lower cover, waste collector, the velocities have opposite direction due to deceleration of the flow.

An interesting characteristic of this flow is that the sum of the mass flow for any horizontal plan is always nil. This means that the mass flow in the ascending direction, central region, should be the same as the mass flow in the descending direction, region close to the rotor wall. That is shown by Figure 8 where the profile ρV_z is presented for the medium plan of the centrifuge.

Figure 9 shows the separative capacity versus the feeding flow. To obtain this curve, the feeding flow was varied from 175 to 2628 kg/year. It was assumed that different values of feeding flow do not disturb the velocity and temperature fields and a cutting factor $\theta = 0.5$. The assumption of a cutting factor $\theta = 0.5$ represents an optimized performance condition, Jordan (1986). Notice that the separative capacity of the centrifuge increases with the feeding flow until 500 kg/year. At this point δU is 0.97 SWU/year decreasing for larger feeding flow

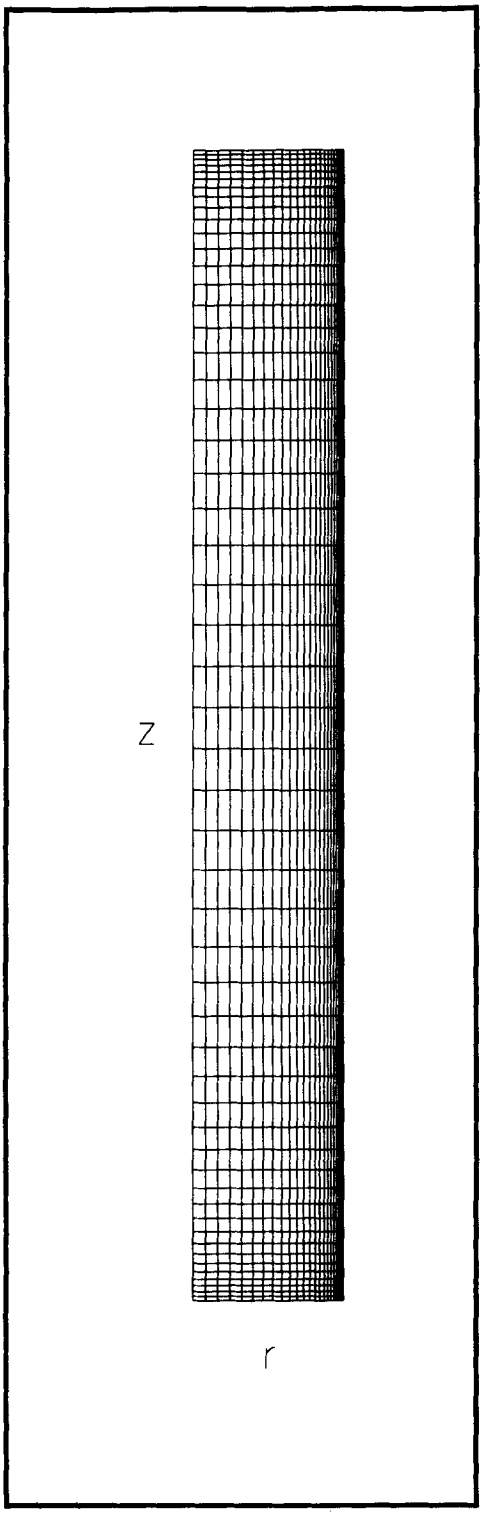

Figure 4 - Typical Mesh

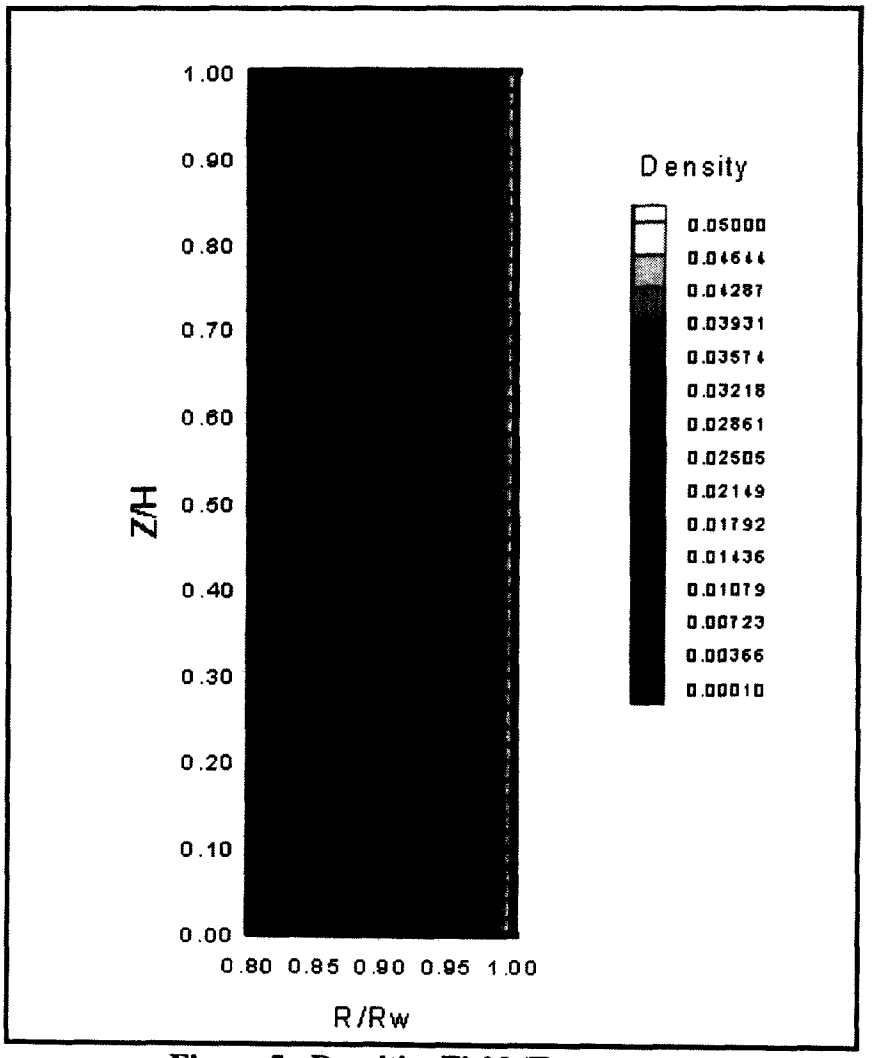

Figure 5 - Densities Field (T=constant)

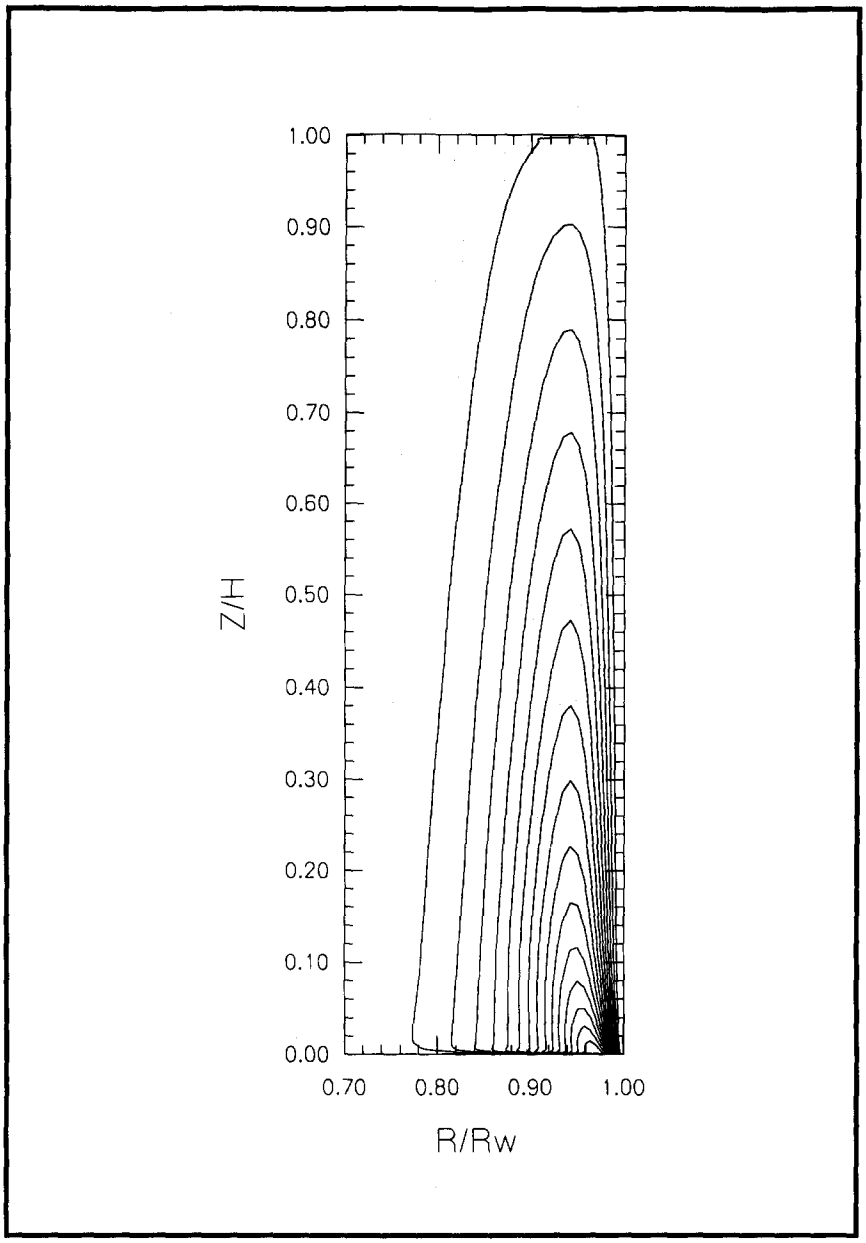

Figure 6 - Stream Lines (T=constant)

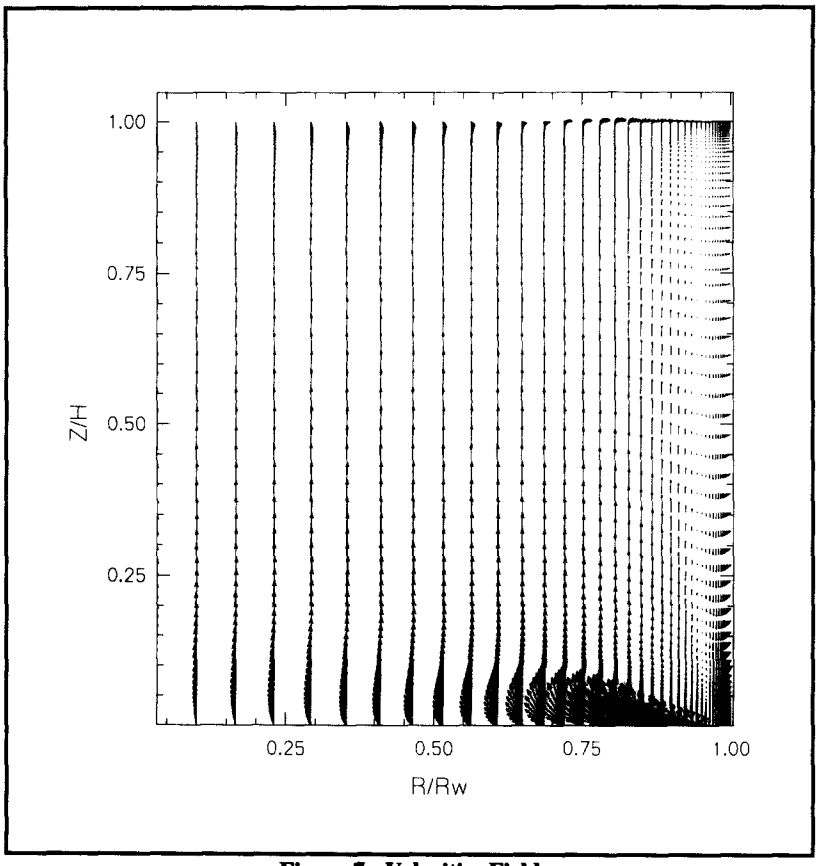

Figure 7 - Velocities Field

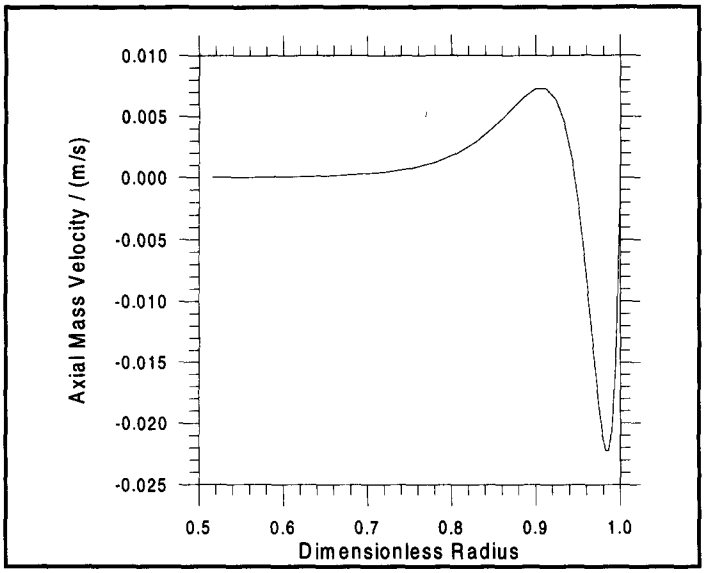

Figure 8 - Axial Mass Velocity Profile X Dimensionless Radius

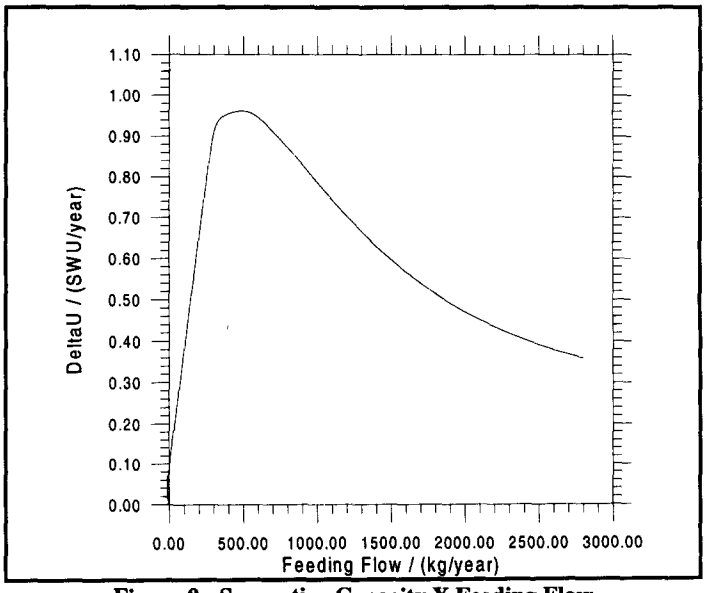

Figure 9 - Separative Capacity X Feeding Flow

values. This curve suggests that the optimum feeding flow for this machine is 500 kg/year where the separative capacity is maximum.

INFLUENCE OF THE THERMAL COUNTERCURRENT ON THE CENTRIFUGE SEPARATIVE CAPACITY

The thermal countercurrent is generated by the temperature gradient on the rotor walls. A favorable countercurrent is generated when the lower disk is at a higher temperature than the upper disk promoting the natural circulation of the gas inside the rotor. This countercurrent also called "Thermal Drive" promotes a more efficient gas circulation in the diffusion stream changing the separation efficiency.

To analyze the influence of the thermal countercurrent on the centrifuge separative capacity two temperature profiles are considered: a profile favorable to the thermal countercurrent where the upper cover is at 303 K and the lower one at 313 K; and an unfavorable profile where the upper cover is kept at 313 K and the lower cover at 303 K. Figure 10 shows the axial mass velocity profiles for the three configurations. It is observed that the profile favorable to the thermal countercurrent increases the mass velocities in the axial direction. The maximum axial mass velocity without the convective effect is 0.0075 m/s while with the profile favorable to the thermal countercurrent this value achieves 0.011 m/s. On the other hand, as the integral of the curve must be nil, the minimum value of the curve decreases form -0.022 m/s to -0.035 m/s. The opposite effect is noticed with the unfavorable thermal profile where the maximum and minimum values of the curve are attenuated in comparison with the reference case, no thermal effect.

Figure 11 presents the Separative Capacity for the configurations analyzed. It is observed that the thermal countercurrent improves the performance of the centrifuge for the whole range of feeding flow studied. Considering a feeding flow of 500 kg/year the favorable profile gives a δU of 1.26 SWU/year which is about 30 % higher than the reference case. In the opposite, the unfavorable profile decreases the separative capacity, δU = 0.59 SWU/year, which is about 39 % lower than the reference case. It is also noticed that a favorable temperature distribution leads to a peak of δU moved to the right, i.e., with larger flow feeding. As it was said previously, to have an efficient centrifuge we should have a high separation factor and a high feeding flow.

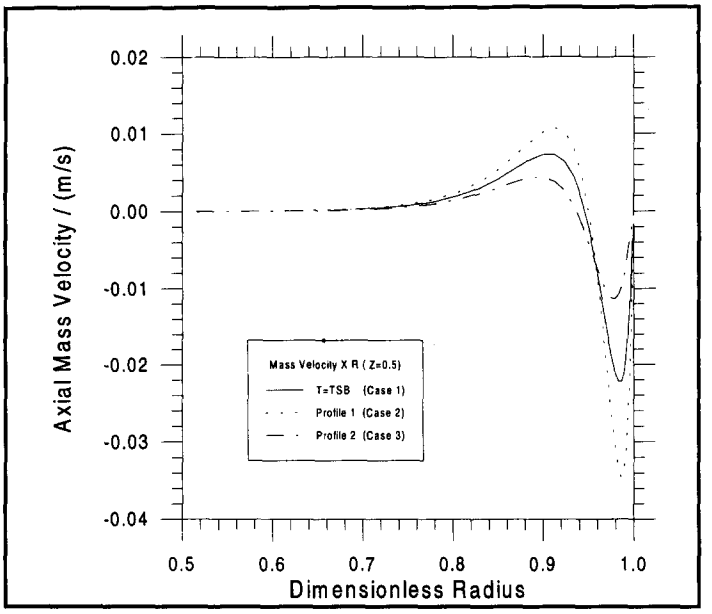

Figure 10 - ρV_z Profile X Dimensionless Radius for the three cases

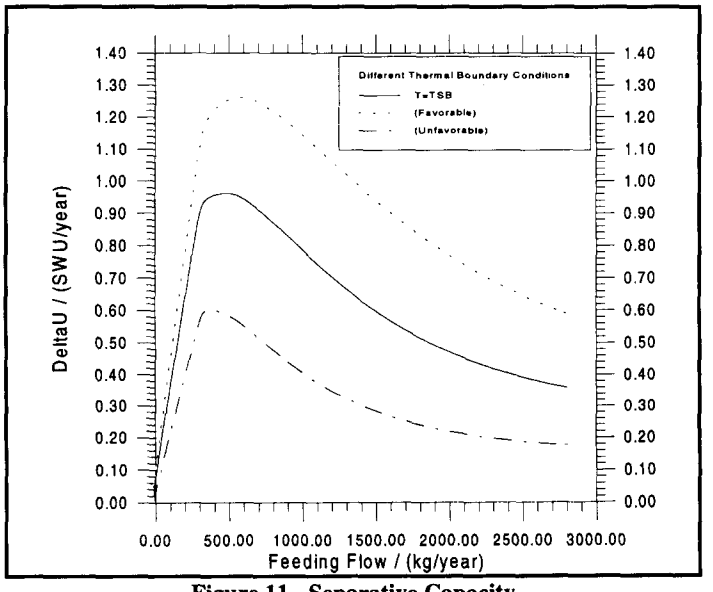

Figure 11 - Separative Capacity

Therefore, the effect of the thermal countercurrent is also positive for moving the peak of the curve to the right.

THERMAL STRUCTURAL MODEL

The results obtained with the hydrodynamical model show that the prediction of the separative capacity of a centrifuge depends on the correct definition of the thermal boundary conditions on the rotor walls. A configuration favorable to the thermal countercurrent increases considerably the separative capacity of the centrifuge, besides it allows the machine to operate with larger flow feeding.

The configurations analyzed in the precedent items were based on arbitrary temperature profiles. It was studied a case where the effect of the thermal countercurrent does not exist, T=TSB, a case where the temperature distribution is favorable to the thermal countercurrent and an unfavorable case. In fact, the rotor temperature distribution depends on the generated heat flows and thermal changes among the several elements that compose the centrifuge. Therefore, to estimate the rotor temperature distribution, a thermal model was developed considering all the relevant heat transfer phenomena:

- heat conduction among the several structural parts;
- radiation in the areas under vacuum;
- natural convection to the environment.

For this analysis the PCTER code, Bastos (1990), was used. This code is composed of four main programs:

GEOTRI - geometric three-dimensional pre-processor responsible for the calculation of the conduction and convection conductances;

GEO - responsible for the calculation of the shape factors for plane geometries;

RAD - responsible for the calculation of the radiative conductances considering the effects of multi reflection among the surfaces using the Gebhart method;

ANATER - it is the main module responsible for the solution of the non-linear algebraic system of equations.

TECPLOT is a commercial code used for post-processing.

Figure 12 is a schematic representation of the centrifuge which was divided into blocks. Table 1 is a list of the elements that compose the centrifuge considered. In the model, a block can be a simple element of the

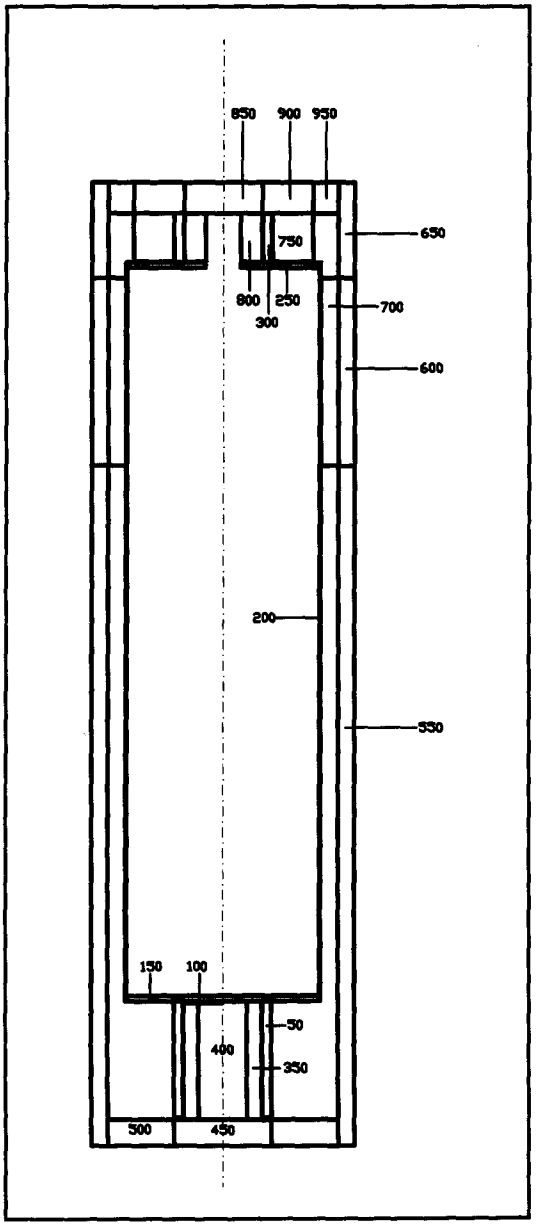

Figure 12 - Thermal Model Geometry

BLOCK	ELEMENT
50	Lower rotor (motor)
100	Lower end cap part- Internal cylinder
150	Lower end cap part- Internal cylinder
200	Internal cylinder
250	Upper end cap part- Internal cylinder
300	Upper end cap part- Internal cylinder
350	Motor wiring
400	Motor core
450	Lower end cap part- Shell
500	Lower end cap part- Shell
550	Shell part
600	Shell part
650	Shell part
700	Molecular pump
750	Axial bearing
800	Upper bearing part
850	Upper end cap part- Shell
900	Upper end cap part- Shell
950	Upper end cap part- Shell

Table 1 - Elements list for the modeled centrifuge

centrifuge, as block 700, turbomolecular pump. It can also represent a complex element as block 400, motor, that is composed of different materials. In this case, the equivalent thermal conductivities are estimated for each direction considering the different materials that compose this block. The properties of the involved materials were taken from Siegel (1972) and Özisik (1985). From the geometric representation in blocks, the program GEOTRI is used to generate the computational mesh.

Figure 13 shows the nodal division used. In Figure 13(a) , the motor (blocks 350 and 400) and the lower cover of the shell (blocks 450 and 500) are represented. Figure 13(b) shows an assembly of the motor, lower cover of the shell, rotor of the motor (block 50) and the lower cover of the cylinder (blocks 100 and 150). Figure 13(c) represents the same blocks of the Figure 13(b) added of the cylinder (block 200) and of the upper cover of the cylinder (blocks 250 and 300). Notice that the cylinder lateral wall, block 200, was divided into several nodes to obtain a larger precision in the indication of the temperature gradient. Figure 13(d) is Figure 13(c) plus the shell upper cover (blocks 850, 900 and 950). Finally, the complete model is shown in Figure 13(e). A wire frame representation of the shell (blocks 450, 500, 550, 600, 650, 850, 900 and 950), turbomolecular pump (block 700) and axial bearing (block 750) is shown.

Table 2 shows the thermal and optical properties used. Columns 2 and 3, present the conductivity of a material for simple blocks and an equivalent conductivity that considers the different materials for complex blocks.

The main heat sources for this centrifuge model are: motor, molecular pump, axial bearing and the flowing gas in contact with the scoop. Table 3 presents the generated heat flows for each element. Notice that the flow generated by the waste collector is 4 W and for the product collector 2 W. These heat flows are generated by the viscous effects of the flowing gas around the collectors or scoops. The waste collector has a larger generated heat flow due to its position in an area of higher pressure in the flow.

Natural convection is considered between the shell and the environment. A simple heat transfer coefficient was considered based on literature correlations.

The radiative changes between the shell and rotor are calculated regarding the effects of multi reflections between the surfaces which are estimated by the Gebhart Method. The calculation method of the radiative

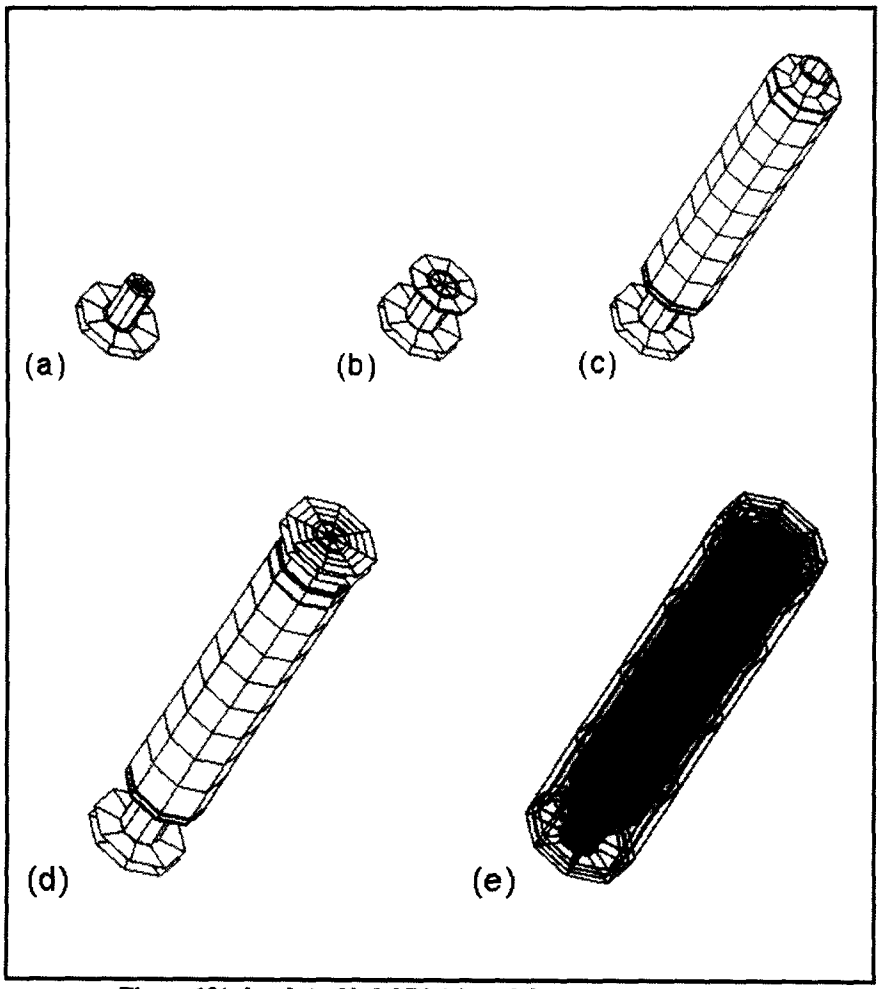

Figure 13(a,b,c,d,e) - Nodal Division of the centrifuge elements

Block	$K_{equivalent}$ / (W/m k)		$\varepsilon = \alpha$
	k_r	k_z	
50	76.11	26.42	0.13
100	20.10	20.10	-
150	20.10	20.10	0.13
200	20.10	20.10	0.60
250	20.10	20.10	-
300	68.72	26.70	-
350	9.34	35.78	-
400	15.00	15.00	-
450	45.00	45.00	-
500	45.00	45.00	0.08
550	45.00	45.00	0.08
600	45.00	45.00	-
650	45.00	45.00	0.08
700	234.0	234.0	0.50
750	10.82	43.89	0.20
800	10.13	5.58	-
850	45.00	45.00	-
900	45.00	45.00	-
950	45.00	45.00	0.08

Table 2 - Materials Thermal and Optical Properties

Block/Node	Heat fluxes / (Watts)
200/202	4
200/211	2
350/350	15
400/400	5
700/700	5
750/750	5

Table 3 - Heat Fluxes

conductances depends on the existence or not of blockage between two surfaces. If there is no blockage, the view factors are calculated by the Boundary Integration Method. If a blockage is present the code uses the Double Discretization Method.

RESULTS OF THE THERMAL MODEL

Case 1: Reference case

Figure 14(a) shows the temperature distribution for the cylinder. The temperature of the motor and lower cover is approximately 62 °C, and it is the cylinder hottest region. That region is close to the largest dissipation.

The gradient on the lateral wall is of the order of 23 °C. The temperature on the lateral wall is 62 °C on the lower part and it decreases to approximately 35 °C on the central region and it grows slightly on the upper third of the cylinder reaching 39 °C on the upper plate. This temperature increase on the upper region is due to the heat flow generated in the product scoop and turbomolecular pump region. It is interesting to observe that this temperature distribution on the rotor wall is quite different from that adopted for the hydrodynamical model.

Figure 14(b) shows the temperature distribution for the shell. The lateral wall temperatures of the shell are close to the ambient temperature. The lower area presents slightly higher temperatures because it is closer to the area of the largest dissipation.

Figure 14(c) shows the temperature distribution for the lower shell cover. The cover central area presents the largest temperature due to the contact with the motor.

In a general way it is observed that:

The lower area presents the largest temperatures because the largest dissipations are in this area.

The heat generated by the motor and scoops is removed mainly by radiation between rotor and shell and rotor and shell and then by natural convection to the ambient.

The temperature difference between the lower and upper covers of the rotor is of 23 °C favoring the generation of the thermal countercurrent.

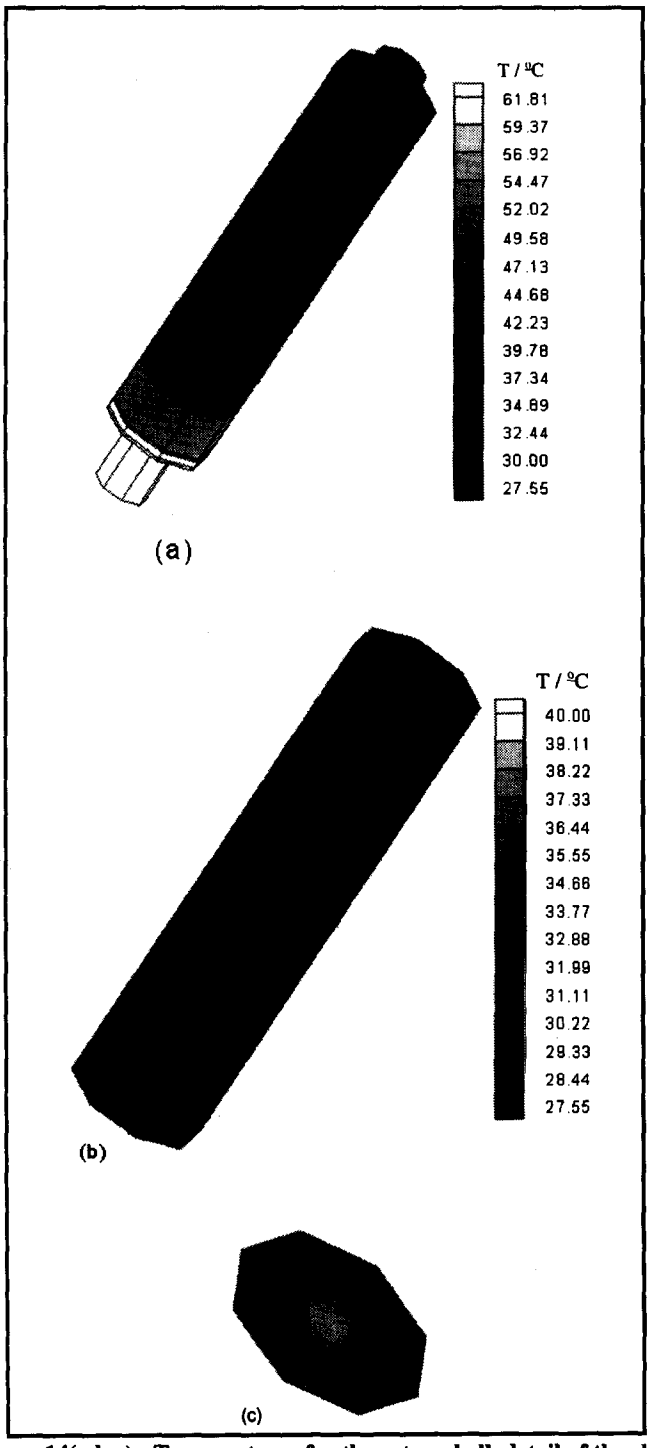

Figure 14(a,b,c) - Temperatures for the rotor, shell, detail of the shell

Case 2: Sensitivity analysis to the materials optical properties

The heat generated by the motor and collectors is mainly removed by radiation between the internal parts and the centrifuge shell. Therefore, acting on the optical properties of the materials, the temperature distribution obtained in case 1 can be altered. This second model refers to a configuration where the material components of the centrifuge were maintained, just optical properties are modified through appropriate thermal and/or chemical treatments. The new values are presented in Table 4. The emissivities of blocks 50, 150 correspond to the steel treated superficially with zinc and chromium. Blocks 200, 500 550, 650 and 950 correspond to the oxidized steel and block 700 to the anodized aluminum.

Figure 15 shows the temperature distribution for the rotor. A decrease of the temperature levels is observed on the rotor due to the best thermal coupling with the shell. Here, the largest rotor temperature, close to the motor area, is 48 ^{o}C. This value is, approximately, 14 ^{o}C lower compared to the same area for case 1. On the other hand, the temperature difference between the lower and upper plates is just 8 ^{o}C against 23 ^{o}C of the previous case. Therefore, this configuration, in spite of decreasing the medium temperature of the centrifuge, also decreases the effect of the convective countercurrent.

CENTRIFUGE SEPARATIVE CAPACITY WITH REAL THERMAL BOUNDARY CONDITIONS

The results obtained with the hydrodynamical model showed the influence of the thermal countercurrent on the separative capacity of the centrifuge. On the other hand, the structural thermal model showed that the real temperature profiles are considerably far from those adopted in the hydrodynamical model. Therefore, it is analyzed here the centrifuge Separative Capacity considering real thermal boundary conditions.

Figure 16 presents a comparison of the centrifuge separative capacity for three different thermal boundary conditions:

1 - No thermal drive (T=TSB);

2 - Thermal boundary condition from the structural thermal model (from Figure 14), corresponding to case 1 in Figure 16;

3 - Thermal boundary condition with modified optical properties (from Figure 15), corresponding to case 2 in

Block	Emissivities
50	0.30
150	0.30
200	0.50
500	0.50
550	0.50
650	0.50
700	0.50
750	0.20
950	0.50

Table 4 - Material Emissivities - Sensitivity Analysis

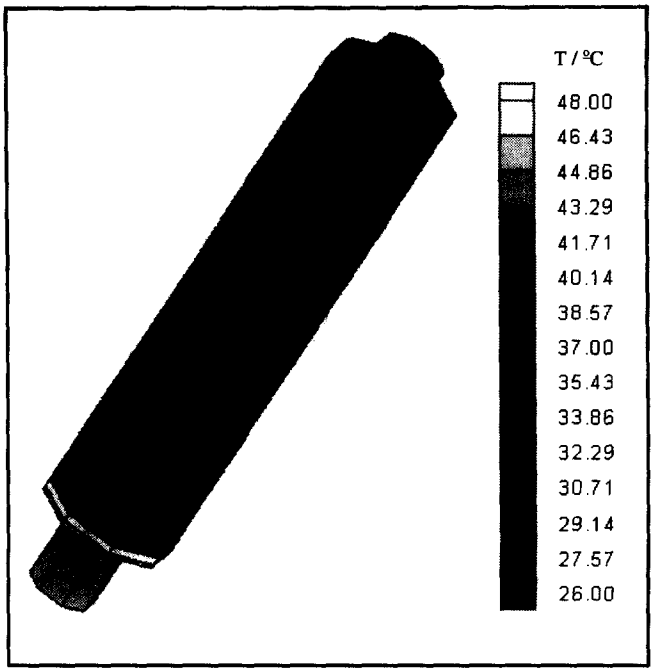

Figure 15 - Sensitivity to the materials optical properties

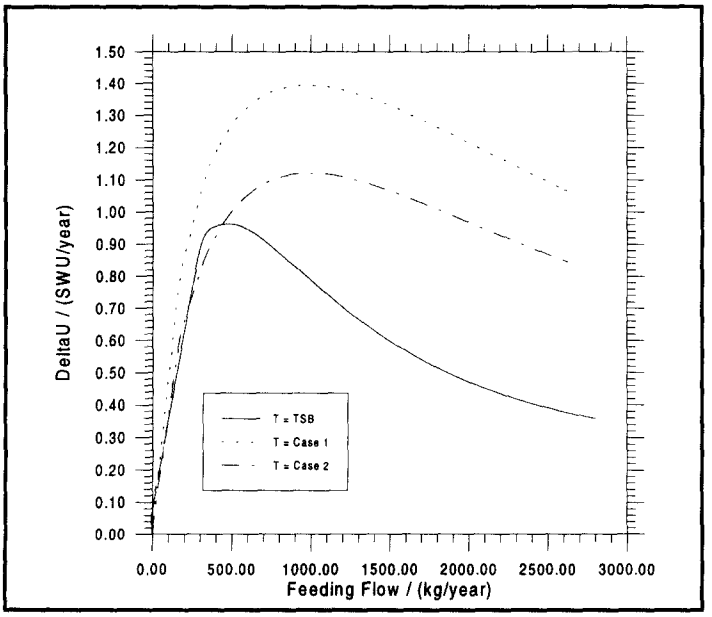

Figure 16 - Separative Capacity X Thermal Boundary Conditions

Figure 16.

It is clear in that the separative capacity is strongly dependent on the thermal boundary conditions as shown in Figure 16.

The dashed curve shows the separative performance of the centrifuge considering the temperature profile shown in Figure 14. It is important to notice that although the average temperature for this in case is larger than that for the other two, it does not necessarily turn out in a worse performance. In this case the thermal countercurrent is pronounced, due to high temperature difference between the covers. The maximum value of δU happens for an approximate feeding flow of 1000 kg/year and it is 1.40 SWU/year.

The point-dashed curve exhibits the corresponding performance for case 2. The maximum value of δU happens for an approximate feeding flow of 1000 kg/year and it is 1.12 SWU/year. The separative capacity is inferior to that for case 1 for the whole feeding flow range analyzed. This result shows that the separative capacity does not necessarily increase with the decrease of the average temperature of operation. For this configuration, the decrease of the average temperature of the centrifuge was accompanied by a decrease of the convective countercurrent provoking the decrease of δU.

The continuous curve exhibits the separative performance for the hypothetical case where the whole rotor is at the temperature TSB. This curve presents a quite different behavior of the two previous confirming the need to use realistic boundary conditions.

Curves referring to cases 1 and 2, Figure 16, present the area of larger separative capacity more sparse, not concentrated as in case of T=TSB. This in practical terms means that it is easier to maintain the equipment working inside its optimal operational range.

FINAL CONCLUSIONS

Hydrodynamical analysis of a countercurrent centrifuge was accomplished where the importance of the thermal boundary condition was verified. A structural thermal model of the centrifuge, considering the main heat transfer phenomena involved was accomplished supplying the hydrodynamical model with realistic thermal boundary conditions.

The procedure adopted, with the thermal and hydrodynamical models integrated, allows a realistic evaluation of the centrifuge separative capacity.

A cost reduction as well as laboratory time reduction is possible using the integrated models, since with the code indications on the separative capacity we can propose modifications on the centrifuge configurations.

References

Bark, F. and Bark, T. H. (1976) *On vertical boundary Layers in a Rapidly Rotating Gas*, Journal of Fluid Mechanics. Vol. 78(4), 749-762;

Bastos, J.L.F.; Muraoka, I. ; Cardoso, H. P. (1990) *Pacote de Análise Térmica - PCTER* - Anais do 1º Simpósio Brasileiro de Tecnologia Aeroespacial, São José dos Campos - SP - Brazil;

Greenspan, H. P. (1969) *Theory of Rotating Fluids*, Cambridge University Press, London;

Jordan, I. (1980) *Separação dos Isótopos de Urânio pelo Processo da Centrifugação em Fase Gasosa.* São Paulo, Instituto de Pesquisas Energéticas e Nucleares - IPEN, IPEN-Inf-3;

Jordan, I. (1986) *Processos de Separação Isotópica do Urânio* - Notas de aula - Curso RNC-741, São Paulo;

Maliska, C.R.; Silva, A.F.; Andrade, D.A. (1992*) A Strong Coupling Procedure for the Segregated Solution of Rotating Flows*, Proceedings of the Third Workshop on Separation Phenomena in Liquids and Gases, page 223-232;

Maliska, C.R. (1995) *Transferência de Calor e Mecânica dos Fluidos Computacional* - Fundamentos e Coordenadas Generalizadas, Rio de Janeiro, Brasil, LTC;

Özisik, M.N., (1985) *Heat Transfer* - A Basic Approach, McGraw-Hill;

Sakurai, T. and Matsuda, T. (1974) *Gasdynamics of a Centrifugal Machine*, Journal of Fluid Mechanics. Vol. 62(4), 727-737;

Siegel, R. ; Howell, J.R., (1972) *Thermal Radiation Heat Transfer*, McGraw-Hill;

Soubbaramayer (1979) *"Centrifugation" - In: Villani*, S.; ed. Uranium Enrichment, Springer Verlag, Berlin;

Stewartson, K. (1957) *On Almost Rigid Rotation*, Journal of Fluid Mechanics. Vol. 3, 17-26;

Zippe, G. (1960) *The Development of Short Bowl Ultra-Centrifuges* - Final Report - Oro 315.